Chemistry–A European Journal
Research Article
doi.org/10.1002/chem.202303185
Chemistry Europe
European Chemical Societies Publishing
www.chemeurj.org

Hot Paper

Stabilization of Diborynes versus Destabilization of Diborenes by Coordination of Lewis Bases: Unravelling the Dichotomy

Lucas de Azevedo Santos[+],*[a] Daniel E. Trujillo-González[+],[b, c] J. Oscar C. Jiménez-Halla,[b] F. Matthias Bickelhaupt,*[a, d, e] and Miquel Solà*[c]

We have quantum chemically investigated the boron-boron bonds in B_2, diborynes B_2L_2, and diborenes $B_2H_2L_2$ (L = none, OH_2, NH_3) using dispersion-corrected relativistic density functional theory at ZORA-BLYP-D3(BJ)/TZ2P. B_2 has effectively a single B–B bond provided by two half π bonds, whereas B_2H_2 has effectively a double B=B bond provided by two half π bonds and one σ 2p–2p bond. This different electronic structure causes B_2 and B_2H_2 to react differently to the addition of ligands. Thus, in B_2L_2, electron-donating ligands shorten and strengthen the boron-boron bond whereas, in $B_2H_2L_2$, they lengthen and weaken the boron-boron bond. The aforementioned variations in boron-boron bond length and strength become more pronounced as the Lewis basicity of the ligands L increases.

Introduction

Metallomimetic elements are the main group elements that mimic the behavior and properties of transition metals (TMs) and, consequently, exhibit similar coordination properties and reactivity as transition metals in coordination complexes.[1–2] Because of the environmental problems, toxicity, high cost, and scarcity associated with many TMs, the chemistry of metallomimetic elements has experienced a surge in interest as prospective substitutes to conventional transition metal-based catalysts and materials. Among the different main group elements with metallomimetic behavior, boron has been probably the most investigated.[3–6] The metallomimetic behavior of boron is observed in different classes of compounds.[7] The two most common are those that combine boron with another nonmetal element like in frustrated Lewis pairs (FLPs)[8–9] and those that have more than one boron center connected by single or multiple B–B bonds like diboranes (B–B), diborenes ($L_2B{=}BL_2$), and diborynes (LB≡BL).[6] FLPs are the most studied boron metallomimetics. They have been applied in catalytic reactions such as the H_2 activation,[10–11] the C–H activation and borylation reactions,[12–14] and in ethene and CO activation.[15–16] On the other hand, the metallomimetic performance of compounds with single or multiple B–B bonds is usually attained by cooperative action of a nucleophilic boron atom or B–B bond and a boron-centered vacant orbital. Diborenes and diborynes can bind small L molecules such as H_2, CO, CO_2, alkynes, or $(CH_3)_2CO$ and activate their bonds in a similar way TMs do.[3,6,17–21]

To stabilize compounds with B–B multiple bonds, it is necessary to fill the vacant $2p_z$ orbital on each boron atom with an electron pair-donating ligand.[6] This is usually achieved by the coordination of σ-donor ligands that act as Lewis bases providing electron density to these electron-deficient species that is supposed to stabilize the B=B double bond in diborenes and the B≡B triple bond in diborynes.[3,22–29] Ideally, stabilization of diborenes and diborynes should not be detrimental for their catalytic activity to activate small molecules.[3,6,17–21] However, if the diborenes and diborynes are strongly stabilized, they may lose their catalytic activity.

In a recent publication, some of us studied the basicity of a series of σ-donor ligands.[30] Our interest was to find optimal σ-donor ligands (L) that stabilize diborenes and diborynes but still keep them catalytically active. Not unexpectedly, we found that the bond dissociation energy of the B≡B triple bond in

[a] Dr. L. de Azevedo Santos,[+] Prof. Dr. F. M. Bickelhaupt
Department of Chemistry and Pharmaceutical Sciences
AIMMS, Vrije Universiteit Amsterdam
De Boelelaan 1108, 1081 HZ Amsterdam (The Netherlands)
E-mail: l.deazevedosantos@vu.nl
f.m.bickelhaupt@vu.nl

[b] D. E. Trujillo-González,[+] Prof. Dr. J. O. C. Jiménez-Halla
Departamento de Química
División de Ciencias Naturales y Exactas
Unversidad de Guanajuato
Noria Alta S/N Col. Noria Alta, Guanajuato, C.P. 36050, Gto. (Mexico)

[c] D. E. Trujillo-González,[+] Prof. Dr. M. Solà
Institut de Química Computacional i Catàlisi and Departament de Química
Universitat de Girona
C/ Maria Aurèlia Capmany, 69, 17003 Girona, Catalonia (Spain)
E-mail: miquel.sola@udg.edu

[d] Prof. Dr. F. M. Bickelhaupt
Institute for Molecules and Materials, Radboud University
Heyendaalseweg 135, 6525 AJ Nijmegen (The Netherlands)

[e] Prof. Dr. F. M. Bickelhaupt
Department of Chemical Sciences
University of Johannesburg
Auckland Park, Johannesburg 2006 (South Africa)

[+] These authors contributed equally to this work.

Supporting information for this article is available on the WWW under https://doi.org/10.1002/chem.202303185

diborynes B_2L_2 increases with the basicity of the σ-donor ligand.[30] Surprisingly, however, we found the opposite behavior for the B=B double bond in diborenes, $B_2H_2L_2$, i.e., stronger Lewis bases reduce the bond dissociation energy of the B=B double bond. As an example, at the PBE0-D3(BJ)/TZ2P level of theory, the gas-phase bond dissociation energy of the B≡B triple bond in B_2L_2 increases from 117.4 to 141.4 kcal mol^{-1} when going from L = NH_3 to a stronger σ-donor like L = CAAC. On the contrary, for the B=B double bond in $B_2H_2L_2$, the B–B bond dissociation energy decreases from 139.7 (L = NH_3) to 92.9 (L = CAAC) kcal mol^{-1} (unpublished results). A complete understanding of the role of σ-donor ligands in the stabilization of B–B multiple bonds is still lacking.[31–32]

With this in mind, the main aim of the present study is to understand the different effects that σ-donor ligands have when coordinated to diborenes and diborynes. To this end, we have quantum chemically analyzed the B–B bond in B_2, B_2H_2, B_2L_2, and $B_2H_2L_2$ (L = H_2O and NH_3), using quantitative Kohn-Sham molecular orbital theory. We anticipate here that B_2 and B_2H_2 respond to the coordination of Lewis base ligands in opposed ways due to their distinct electronic structures. In B_2L_2, electron-donating ligands shorten and strengthen the boron-boron bond. In contrast, in $B_2H_2L_2$, they lengthen and weaken the boron-boron bond.

Results and Discussion

Structure and bond strength

Equilibrium geometries, bond energies (Δ*E*), and B–B bond lengths ($r_{B\text{-}B}$) of $B_2^{\bullet\bullet}$ and $B_2H_2^{\bullet\bullet}$ and *trans* B_2L_2 and $B_2H_2L_2$ (L = H_2O and NH_3) calculated at the ZORA-BLYP-D3(BJ)/TZ2P[33–37] level of theory are shown in Figure 1 (the Cartesian coordinates for all stationary points are given in Table S2). $B_2H_2L_2$ exists in *cis* and in the most stable *trans* configuration, which is the one we analyze here.[38] First, we find that the B–B bond becomes stronger and shorter when going from the diborane in its triplet ground state ($B_2^{\bullet\bullet}$)[39] to the diborene in its triplet ground state ($B_2H_2^{\bullet\bullet}$). For example, from $B_2^{\bullet\bullet}$ to $B_2H_2^{\bullet\bullet}$, Δ*E* varies from −67.8 kcal mol^{-1} to −173.0 kcal mol^{-1} and $r_{B\text{-}B}$ varies from 1.618 Å to 1.514 Å (Figure 1). These results for B_2 and B_2H_2 are in agreement with those obtained experimentally or with high-level calculations. For example, the experimental bond dissociation energy for the diboron molecule in its $^3\Sigma_g^-$ ground state is 65.5 ± 5.5[40] and the experimental bond length is 1.590 Å.[41] This bond length was computed to be 1.586 Å and 1.593 Å at the UCCSD(T)-F12b and MR-CISD levels, respectively.[42] Structural and thermochemical information in the diborene parent compound B_2H_2 is scarce. B_2H_2 is a linear molecule of $D_{\infty h}$ symmetry and a $^3\Sigma_g^-$ ground state.[43–45] Bond lengths $r_{B\text{-}B}$ of 1.514 Å and 1.507 Å were computed for the $^3\Sigma_g^-$ state at the CAS-MRCI[46] and MRCI + Q[47] levels of theory, respectively.

Next, we find that $B_2^{\bullet\bullet}$ and $B_2H_2^{\bullet\bullet}$ behave differently with the addition of ligands to form the B_2L_2 and $B_2H_2L_2$ in their singlet ground states, respectively. That is, the B–B bond becomes stronger and shorter from $B_2^{\bullet\bullet}$ to B_2L_2, but weaker and longer from $B_2H_2^{\bullet\bullet}$ to $B_2H_2L_2$. In both cases, the effect is more pronounced for the σ-donor ligand with higher basicity (L = NH_3). For example, in the series of $B_2^{\bullet\bullet}$, $B_2(OH_2)_2$, $B_2(NH_3)_2$, Δ*E* varies along −67.8 kcal mol^{-1}, −88.0 kcal mol^{-1}, and −112.6 kcal mol^{-1} and $r_{B\text{-}B}$ varies along 1.618 Å, 1.499 Å, and 1.452 Å (Figure 1). In the series of $B_2H_2^{\bullet\bullet}$, $B_2H_2(OH_2)_2$, $B_2H_2(NH_3)_2$, Δ*E* varies along −173.0 kcal mol^{-1}, −147.1 kcal mol^{-1}, and

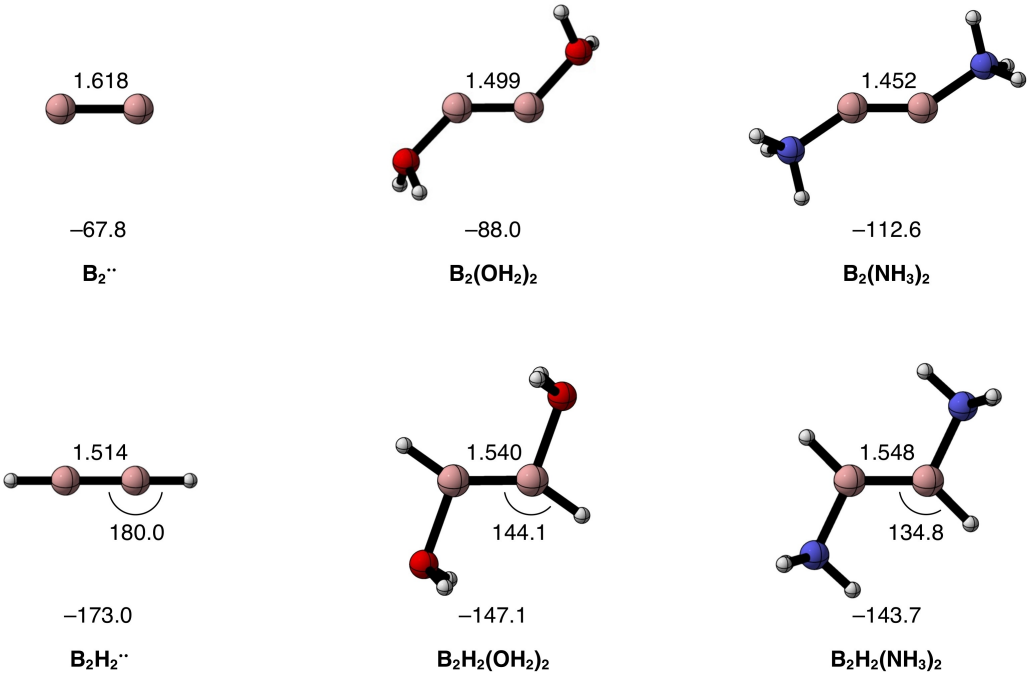

Figure 1. Equilibrium geometries (in Å and deg.) and electronic homolytic bond dissociation energies (in kcal mol^{-1}) of the B–B bonds in $B_2^{\bullet\bullet}$, $B_2(OH_2)_2$, $B_2(NH_3)_2$, $B_2H_2^{\bullet\bullet}$, $B_2H_2(OH_2)_2$, and $B_2H_2(NH_3)_2$. Computed at ZORA-BLYP-D3(BJ)/TZ2P.

−143.7 kcal mol^{-1} and $r_{B\text{-}B}$ varies along 1.514 Å, 1.540 Å, and 1.548 Å. As a result, the B–B bond in B_2L_2 is much weaker than in $B_2H_2L_2$ by 59.1 kcal mol^{-1} for L=H_2O and 31.1 kcal mol^{-1} for L = NH_3, similar to the case of $B_2^{••}$ and $B_2H_2^{••}$. But, unexpectedly from bond dissociation energies, the B–B bond in B_2L_2 is much shorter than in $B_2H_2L_2$. This result is in agreement with the reported shorter B–B bond distance for $B_2(CAAC)_2$ than for $B_2H_2(CAAC)_2$.[48] In the coming sections, we explain these observations.

$B_2^{••}$ versus $B_2H_2^{••}$

In this section, we analyze the electronic structure of $B_2^{••}$ and $B_2H_2^{••}$ and explain why the B–B bond is stronger and shorter in the latter. To this end, we analyze the formation of $B_2H_2^{••}$ by the reaction between $B_2^{••}$ and H_2 in its singlet ground state (Scheme 1a). The electronic structure of $B_2^{••}$ is a textbook example of a diatomic molecule. Scheme 2a shows the molecular orbital diagram corresponding to the formation of $B_2^{••}$ from two B atoms. From Li_2 to N_2, the degenerate $1\pi_u$ molecular orbitals (MOs) are lower in energy than the $3\sigma_g$ MO. This is because of the s-p orbital mixing in the $2\sigma_g$ and $3\sigma_g$ MOs, which stabilizes the $2\sigma_g$ MOs of $B_2^{••}$ and destabilizes the $3\sigma_g$ MO of $B_2^{••}$.[49] As a consequence, the $1\pi_u$ MOs of $B_2^{••}$ are singly occupied and the $3\sigma_g$ MO of $B_2^{••}$ is empty, according to Hund's rule. Therefore, $B_2^{••}$ has two half π-bonds and a triplet ground state.[49]

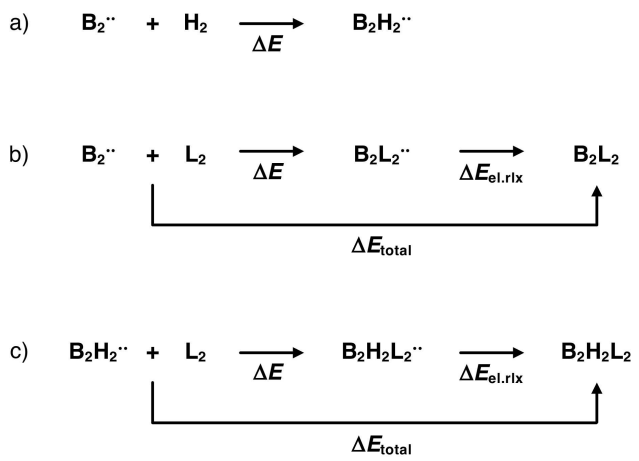

Scheme 1. Stepwise formation of a) $B_2H_2^{••}$, b) B_2L_2, and c) $B_2H_2L_2$ (L=OH_2, NH_3) from the core $B_2^{••}$ and $B_2H_2^{••}$ molecules.

The addition of the singlet H_2 fulfills the empty $3\sigma_g^0$ MO of $B_2^{••}$, and the final valence MO configuration of $B_2H_2^{••}$ is $2\sigma_g^2 2\sigma_u^2 3\sigma_g^2 1\pi_{u,x}^1 1\pi_{u,y}^1$. This configuration is also the leading MRCI configuration for the ground state of this system with a coefficient of 0.97.[47] Consequently, $B_2H_2^{••}$ has a complete σ bond in addition to the same two half π-bonds of $B_2^{••}$, that is, $B_2H_2^{••}$ has a boron-boron double bond, whereas $B_2^{••}$ has a boron-boron single bond. For this reason, the B–B bond is stronger in the former, albeit, as will become clear in the following, it is not yet the reason why the B–B bond becomes shorter in $B_2H_2^{••}$. Scheme 2b shows the MO diagram for the formation of $B_2H_2^{••}$ from $B_2^{••}$ and H_2. As can be seen, there is a stabilizing donor-acceptor interaction between the $3\sigma_g$ acceptor MO of $B_2^{••}$ and the $1\sigma_g$ donor MO of H_2. The main difference between the electron configuration of $B_2^{••}$ and $B_2H_2^{••}$ is that the $3\sigma_g$ MO is empty in the former and fulfilled in the latter.

To understand the shortening of the B–B bond when going from $B_2^{••}$ to $B_2H_2^{••}$, we performed the activation strain analysis[50–51] (ASA) of the interaction between $B_2^{••}$ and H_2 to decompose the bond energies (ΔE) into the strain (ΔE_{strain}) and

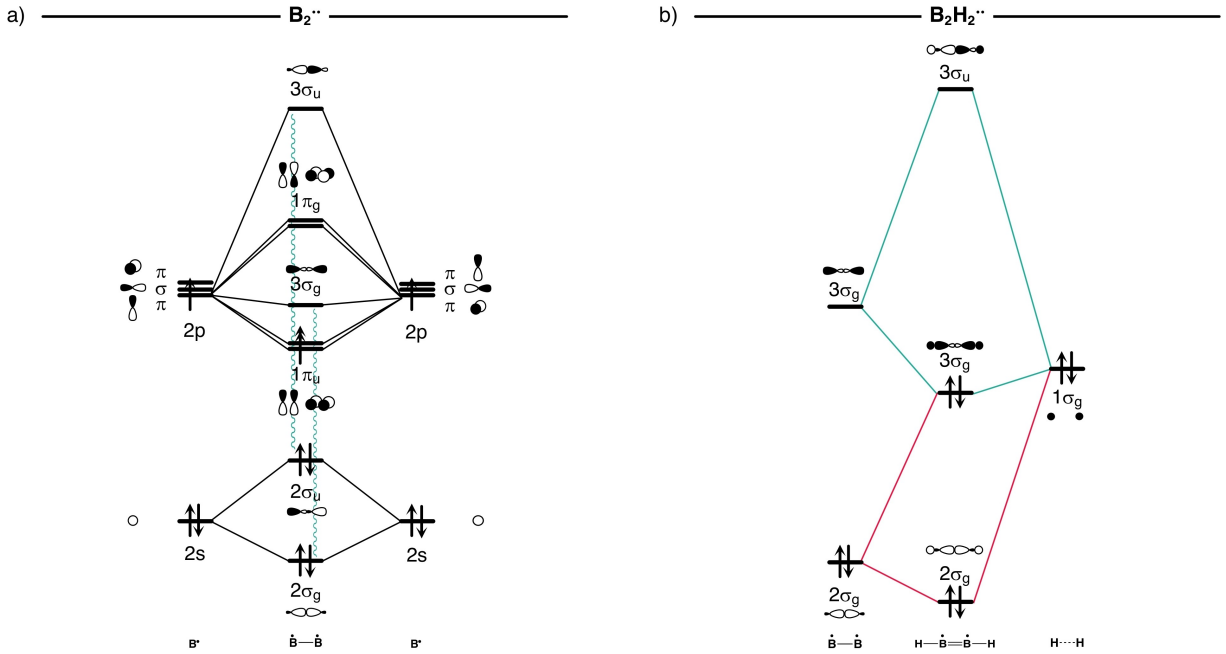

Scheme 2. Schematic valence molecular orbital diagram for the reactions a) B$^•$ + B$^•$ → $B_2^{••}$ and b) $B_2^{••}$ + H_2 → $B_2H_2^{••}$.

interaction ($\Delta E_{int,B2\text{-}H2}$) energies (see Computational Methods). The analysis is performed as a function of the B–B bond distance from $r_{B\text{-}B}$ = 1.4 Å to 1.8 Å, while keeping all bond angles and B–H bond lengths frozen to the equilibrium geometry of $B_2H_2^{••}$ (Figure 2a). The results of all studied systems at their equilibrium geometries can be found in Table S1 of the Supporting Information. First, the $\Delta E(r_{B\text{-}B})$ curve has a soft parabolic profile with an energy minimum around 1.5 Å, which is the equilibrium B–B bond length of $B_2H_2^{••}$. The energy profile of $\Delta E_{strain}(r_{B\text{-}B})$ is similar to $\Delta E(r_{B\text{-}B})$, but the energy minimum is at longer $r_{B\text{-}B}$, around 1.6 Å. This is because the $\Delta E_{strain}(r_{B\text{-}B})$ curve mainly reflects the stability of the $B_2^{••}$ fragment, which $r_{B\text{-}B}$ is 1.618 Å at its equilibrium geometry. In turn, the $\Delta E_{int,B2\text{-}H2}(r_{B\text{-}B})$ curve becomes increasingly more stabilizing as the B–B bond contracts and, thus, shifts the energy minimum to shorter B–B bond lengths, as compared to $B_2^{••}$.

To understand the trends in $\Delta E_{int,B2\text{-}H2}(r_{B\text{-}B})$, we further decomposed the ΔE_{int} into four physically meaningful terms, namely the electrostatic interactions (ΔV_{elstat}), steric Pauli repulsion (ΔE_{Pauli}), orbital interactions (ΔE_{oi}), and dispersion energy (ΔE_{disp}) using our energy decomposition analysis[50–53] (EDA; see Computational Methods). We find that the larger stabilization of $\Delta E_{int,B2\text{-}H2}(r_{B\text{-}B})$ at short B–B bond lengths is due to a significant reduction of the Pauli repulsion curve, $\Delta E_{Pauli}(r_{B\text{-}B})$. When shortening the B–B bond distance, the amplitude of the $2\sigma_g$ MO of $B_2^{••}$ becomes more localized in the bonding regime, reducing the amplitude in the outer regions that overlap with the $1\sigma_g$ occupied MO of H_2. As a result, the $\langle 2\sigma_g(B_2^{••}) \,|\, 1\sigma_g(H_2)\rangle$ overlap diminishes (see Figure S1) and the destabilizing Pauli repulsion between these two occupied MOs decreases. On the other hand, we find that the donor-acceptor interaction between $B_2^{••}$ and H_2 favors the elongation, not contraction, of the B–B bond, as the orbital interactions curve, $\Delta E_{oi}(r_{B\text{-}B})$, becomes more stabilizing as $r_{B\text{-}B}$ increases. This is because of the aforementioned s-p orbital mixing in the $3\sigma_g$ MOs $B_2^{••}$ that increases by shrinking the B–B bond distance and, thus, destabilizes the $3\sigma_g$ unoccupied MO of $B_2^{••}$. As a result, the HOMO-LUMO gap ($\Delta\varepsilon$) between the $3\sigma_g$ of $B_2^{••}$ and the $1\sigma_g$ of H_2 increases (see Figure S1), reducing significantly the favorable orbital interaction. However, this more favorable orbital interaction as the B–B bond elongates is not enough to overcome the favorable Pauli repulsion lowering effect as the B–B bond shortens.

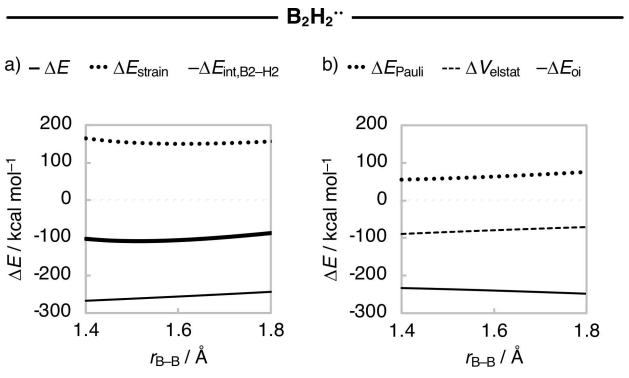

Figure 2. a) Activation strain and b) energy decomposition analyses (in kcal mol^{-1}) as a function of the B–B bond length for the interaction between $B_2^{••}$ and H_2, while keeping the B–H moieties frozen at the equilibrium geometry of $B_2H_2^{••}$. Dispersion energy is negligible and, therefore, now shown. Computed at ZORA-BLYP-D3(BJ)/TZ2P.

B_2L_2 versus $B_2H_2L_2$

Now, we address the question: why do $B_2^{••}$ and $B_2H_2^{••}$ behave differently to the addition of ligands? To this end, we analyze the formation of B_2L_2 and $B_2H_2L_2$ by the reaction of $B_2^{••}$ and $B_2H_2^{••}$ with L_2 in two steps (Scheme 1b and 1c). In the first step, $B_2^{••}$ and $B_2H_2^{••}$ react with L_2, yielding $B_2L_2^{••}$ and $B_2H_2L_2^{••}$ in their triplet excited state, in the equilibrium geometry of B_2L_2 and $B_2H_2L_2$. Later on, $B_2L_2^{••}$ and $B_2H_2L_2^{••}$ are allowed to relax, yielding B_2L_2 and $B_2H_2L_2$ in their singlet ground state. As will become clear in the following, the difference in the behavior of $B_2^{••}$ and $B_2H_2^{••}$ when interacting with σ-donor ligands is due to the different nature of the acceptor MOs of $B_2^{••}$ and $B_2H_2^{••}$, which is a σ B–B bonding MO in the former and a π* B–B antibonding MO in the latter.

Scheme 3a depicts the MO diagram for the interaction between $B_2^{••}$ and L_2 to form $B_2L_2^{••}$. Similar to the formation of $B_2H_2^{••}$ (Scheme 3a), the formation of $B_2L_2^{••}$ occurs via a donor-acceptor interaction between $B_2^{••}$ and L_2. That is, in $B_2L_2^{••}$, the initial empty $3\sigma_g$ B–B bonding MO of $B_2^{••}$ is fulfilled, resulting in the formation of an additional, σ B–B bond (Scheme 3a). However, differently from $B_2H_2^{••}$, L_2 has four electrons coming from two σ lone-pair orbitals (σ_{LP} and σ^*_{LP}), two electrons more than H_2. Therefore, $B_2L_2^{••}$ experiences the additional two center three electron interaction between the singly occupied $1\pi_{u,x}$ MO of $B_2^{••}$ and the σ^*_{LP} of L_2. On one hand, it fulfills the $1\pi_{u,x}$ MO of $B_2^{••}$, resulting in an additional half π B–B bond. On the other hand, one radical of $B_2^{••}$ is significantly pushed up (i.e., is destabilized) by the Pauli repulsion between the $1\pi_{u,x}$ MO of $B_2^{••}$ and the σ^*_{LP} of L_2. For this reason, this excited radical can easily drop to and fulfill the lower-lying singly occupied $1\pi_{u,y}$ MO of $B_2^{••}$, yielding B_2L_2 (see green arrow in Scheme 3a). Consequently, in $B_2L_2^{••}$ the initial $3\sigma_g$ and $1\pi_u$ orbitals of $B_2^{••}$ are filled causing the strengthening and shortening of the B–B bond, which acquires triple bond character.

The formation of $B_2H_2L_2^{••}$ also occurs via a donor-acceptor interaction between $B_2H_2^{••}$ and L_2. Nevertheless, contrary to $B_2^{••}$, the $3\sigma_g$ MO of $B_2H_2^{••}$ already fulfilled and cannot accept electrons from L_2. Alternatively, in $B_2H_2L_2^{••}$, L_2 donates charge from its σ_{LP} orbital into the empty $1\pi_g$ B–B antibonding MO, causing the weakening of the B–B bond and reducing the double bond character of $B_2H_2^{••}$ when forming $B_2H_2L_2^{••}$ (Scheme 3b). Note that, in MO theory, filling the B–B antibonding molecular orbital translates into the increase of Pauli repulsion and, thus, the lengthening of the B–B bond. Similar to $B_2L_2^{••}$, the singly occupied $1\pi_{u,x}$ MO of $B_2H_2^{••}$ also accepts charge from the σ^*_{LP} of L_2, which causes the significant destabilization of the $1\pi_{u,x}$ $B_2H_2^{••}$ radical by Pauli repulsion. Again, this excited radical drops and fulfills the lower-lying singly occupied $1\pi_{u,y}$ MO of $B_2H_2^{••}$, yielding $B_2H_2L_2$ (see green arrow in Scheme 3b).

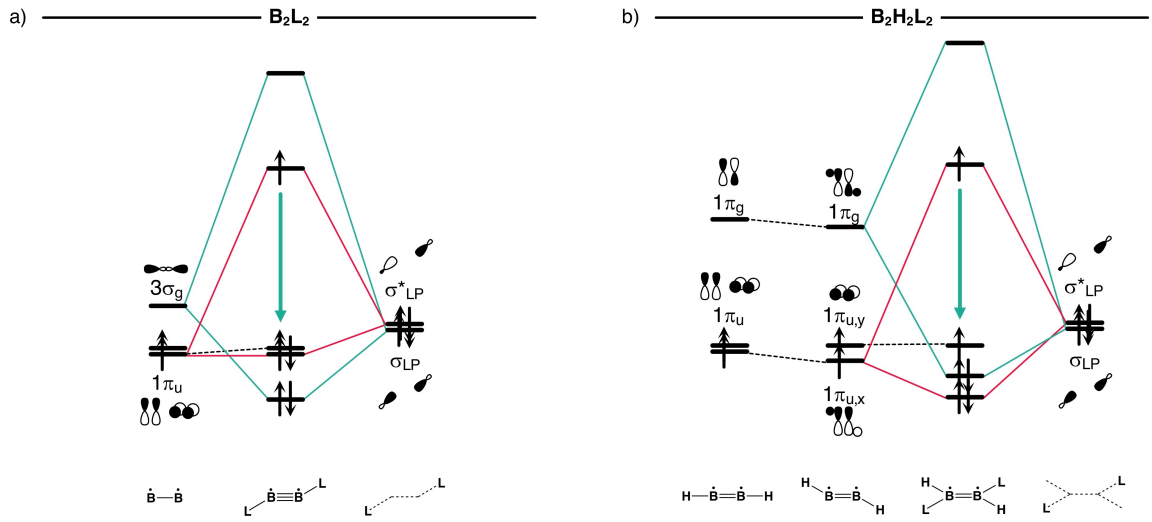

Scheme 3. Schematic molecular orbital diagram for the reactions a) $B_2^{\bullet\bullet} + L_2 \rightarrow B_2L_2^{\bullet\bullet}$ and b) $B_2H_2^{\bullet\bullet} + L_2 \rightarrow B_2H_2L_2^{\bullet\bullet}$.

Alkorta et al.[38] also found that stronger σ-donor ligands lead to longer B–B bond distances in $B_2H_2L_2$ species.

In short, the donor-acceptor interactions between B–B bonds and σ-donor ligands strengthen the B–B bond in $B_2^{\bullet\bullet}$ and weakens the B–B bond in $B_2H_2^{\bullet\bullet}$. These effects become more pronounced when increasing the Lewis basicity of L_2. For this reason, the B–B bond becomes increasingly stronger and shorter along $B_2^{\bullet\bullet}$, $B_2(OH_2)_2$, and $B_2(NH_3)_2$, but increasingly weaker and longer along $B_2H_2^{\bullet\bullet}$, $B_2H_2(OH_2)_2$, and $B_2H_2(NH_3)_2$. This emerges from our analyses of the interaction between $B_2^{\bullet\bullet}$ and L_2 and between $B_2H_2^{\bullet\bullet}$ and L_2 as a function of the B–B bond distance from $r_{B\text{-}B}$ = 1.4 Å to 1.8 Å, while keeping all bond angles and B–H and B–L bond lengths frozen to the equilibrium geometry of B_2L_2 and $B_2H_2L_2$ (L = OH_2, NH_3; Figure 3). Herein, we decompose the total bonding energy for the reaction of $B_2^{\bullet\bullet}$ and $B_2H_2^{\bullet\bullet}$ with L_2 (ΔE_{total}) into two components: (i) ΔE is the energy associated with the L_2 addition step to form $B_2L_2^{\bullet\bullet}$ and $B_2H_2L_2^{\bullet\bullet}$; and (ii) $\Delta E_{el.rlx}$ is the energy associated to the electronic relaxation from the triplet excited states to the singlet ground states, that is, from $B_2L_2^{\bullet\bullet}$ and $B_2H_2L_2^{\bullet\bullet}$ to B_2L_2 and $B_2H_2L_2$ (see Scheme 1b and 1c). Next, we perform the ASA to decompose ΔE into ΔE_{strain} and $\Delta E_{int,B2\text{-}L2}$, and the results are graphically shown in Figure 3a.

For both B_2L_2 and $B_2H_2L_2$, the $\Delta E_{total}(r_{B\text{-}B})$ curves become more stabilizing from L= OH_2 to NH_3 (Figure 3a). This is due to the more stabilizing $\Delta E_{int,B2\text{-}L2}(r_{B\text{-}B})$ for the stronger σ-donor NH_3 ligand. The energy minimum is shifted towards shorter B–B bond lengths for B_2L_2, whereas the energy minimum is shifted towards longer B–B bond lengths for $B_2H_2L_2$. This is because the slopes of the $\Delta E_{int,B2\text{-}L2}(r_{B\text{-}B})$ curves are different for B_2L_2 and $B_2H_2L_2$. That is, as the B–B bond contracts, the $\Delta E_{int,B2\text{-}L2}(r_{B\text{-}B})$ curves have a descending slope for B_2L_2, but an ascending one for $B_2H_2L_2$. In addition, the slopes of the $\Delta E_{int,B2\text{-}L2}(r_{B\text{-}B})$ curves are larger for L = NH_3, resulting in a shorter B–B bond for $B_2(NH_3)_2$ and a longer B–B bond for $B_2H_2(NH_3)_2$.

The reason for the behavior of $\Delta E_{int,B2\text{-}L2}(r_{B\text{-}B})$ for different L is the magnitude and slope of the $\Delta E_{oi}(r_{B\text{-}B})$ curves that becomes more stabilizing and steeper along L = OH_2 to NH_3 (Figure 3b). As we already mentioned, in B_2L_2, the ligands donate charge from their σ lone-pair orbitals into the empty $3\sigma_g$ B–B bonding

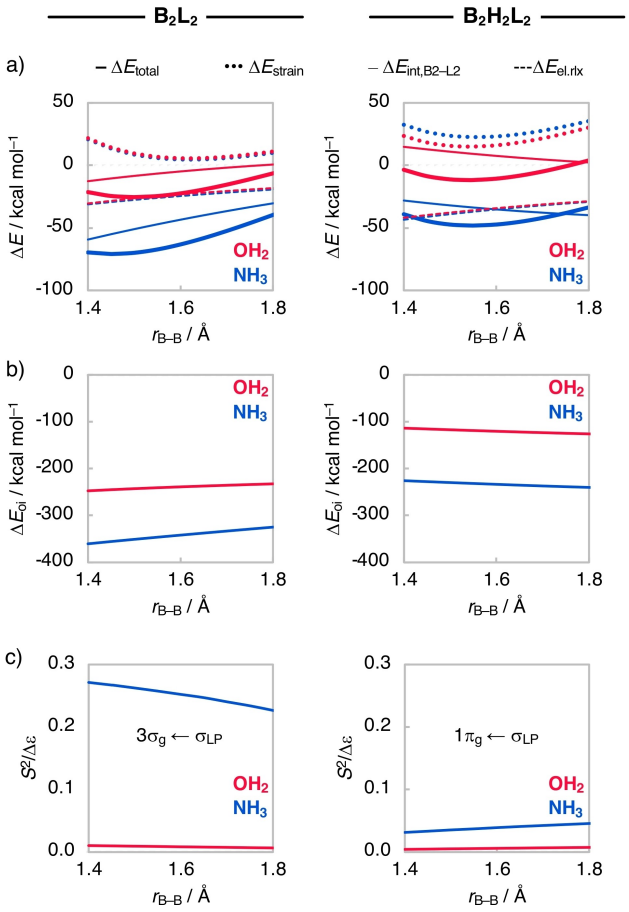

Figure 3. a) Activation strain analysis (in kcal mol^{-1}), b) orbital interactions energy (in kcal mol^{-1}), and c) orbital stabilization as a function of the B–B bond length for the interaction between $B_2^{\bullet\bullet}$ or $B_2H_2^{\bullet\bullet}$ and L_2 (L=OH_2, NH_3), while keeping the B(H)L moieties frozen at the equilibrium geometry of $B_2(H_2)L_2$. Computed at ZORA-BLYP-D3(BJ)/TZ2P.

MO of $B_2^{••}$. Due to the s-p orbital mixing, the amplitude of the empty $3\sigma_g$ bonding MO of $B_2^{••}$ becomes more localized in the outer regions as the B–B bond contracts (see Scheme 3a), resulting in an increased $\langle 3\sigma_g(B_2^{••}) \mid \sigma_{LP}(L_2)\rangle$ overlap and, thus, more stabilizing ΔE_{oi} at shorter B–B bonds. The σ lone-pair orbitals of NH_3 are higher in energy and more diffuse than the σ lone-pair orbitals of OH_2, resulting in a smaller HOMO-LUMO gap (Δε) and larger stabilizing orbital overlap (S) and, thus, more stabilizing ΔE_{oi} (Figure S3). We recall that the relevance of a donor-acceptor interaction can be estimated by the magnitude of its orbital stabilization which is proportional to its HOMO-LUMO overlap squared (S^2) divided by its respective orbital energy gap ($\Delta\varepsilon$). This means that donor-acceptor interactions are more sensitive to variations for larger S^2 and for smaller $\Delta\varepsilon$ and, for this reason, the $\Delta E_{oi}(r_{B\text{-}B})$ curves descend faster when shortening the B–B bonds for L = NH_3 (Figure 3c).

In $B_2H_2L_2$, the ligands donate charge from their σ lone-pair orbitals into the empty $1\pi_g$ B–B antibonding MO of $B_2H_2^{••}$. Therefore, the $1\pi_g$ MO of $B_2H_2^{••}$ is stabilized and goes down in energy as the B–B bond elongates, resulting in a smaller $\Delta\varepsilon$ and, thus, more stabilizing ΔE_{oi}. Note that $\Delta\varepsilon$ is smaller for the stronger Lewis base, σ-donor NH_3 compared to H_2O (Figure S3). Therefore, the orbital stabilization is more sensitive to $r_{B\text{-}B}$ and the $\Delta E_{oi}(r_{B\text{-}B})$ curves descend faster when elongating the B–B bond for L = NH_3 (Figure 3c).

Conclusions

We have quantum chemically analyzed the boron-boron bonds in $B_2^{••}$, $B_2H_2^{••}$, diborynes B_2L_2, and diborenes $B_2H_2L_2$ (L=OH_2, NH_3) using Kohn–Sham molecular orbital theory at the ZORA-BLYP-D3(BJ)/TZ2P level. We find that the effective single B–B bond in $B_2^{••}$ is weaker and longer than the effective double B=B bond in $B_2H_2^{••}$. The coordination of Lewis bases to these B–B bonds via HOMO-LUMO interactions stabilizes the diborynes B_2L_2 but destabilizes the diborenes $B_2H_2L_2$. Our results show that ligands with a stronger Lewis basicity further strengthen and contract the B–B bond in $B_2^{••}$ but weaken and elongate the B–B bond in $B_2H_2^{••}$. This is because of the different nature of the acceptor orbitals, that is a σ B–B bonding orbital in $B_2^{••}$ and a π* B–B antibonding orbital in $B_2H_2^{••}$. As such, strong σ-donor ligands induce the formation of a B–B multiple bond in B_2L_2 but decrease the B=B double bond character in $B_2H_2L_2$. Interestingly, the B–B bond distance in B_2L_2 is shorter but the dissociation energy remains smaller than in $B_2H_2L_2$. We expect that stronger σ-donors than NH_3 may result in a B–B bond dissociation energy that is larger for B_2L_2 than for $B_2H_2L_2$.

Computational Methods

Computational details

All calculations were performed using the Amsterdam Modeling Suite (AMS) 2022.101 program.[54–55] All stationary points and energies were obtained using relativistic, dispersion-corrected density functional theory at ZORA-BLYP-D3(BJ)/TZ2P[34–35,37,56] (see Table S2 in the Supporting Information for the Cartesian coordinates). All electrons were included in the variational process, i.e., no frozen core approximation was applied. The accuracies of both the fitting scheme and the integration grid (Becke grid) were set to 'EXCELLENT'. All optimized structures were confirmed to be true minima through vibrational analysis (no imaginary frequencies). For each species, we have analyzed only the most stable conformer.

Bond analyses

The bond analyses in $B_2H_2^{••}$, B_2L_2, and $B_2H_2L_2$ were performed considering a two-step reaction between $B_2^{••}$ or $B_2H_2^{••}$ and H_2 and L_2 (Scheme 1). In the first step, we consider energy associated with the formation of the products without changing the multiplicity of the reactants, ΔE. In the second step, we consider the electronic relaxation from the excited state of the products to their ground state, $\Delta E_{el.rlx}$. The total energy for the reaction of the combined two steps is ΔE_{total}, [Equation (1)]. If no electronic relaxation occurs, that is, the multiplicity of the products is the same as the reactants, $\Delta E_{total} = \Delta E$.

$$\Delta E_{total} = \Delta E + \Delta E_{el.rlx} \tag{1}$$

The bond energy ΔE is decomposed along the B–B bond distance $r_{B\text{-}B}$ into the strain energy $\Delta E_{strain}(r_{B\text{-}B})$, which is associated with the geometrical deformation of the individual reactants as the process takes place, plus the actual interaction energy $\Delta E_{int}(r_{B\text{-}B})$ between the deformed reactants [Equation (2)].

$$\Delta E(r_{B\text{-}B}) = \Delta E_{strain}(r_{B\text{-}B}) + \Delta E_{int}(r_{B\text{-}B}) \tag{2}$$

In the equilibrium geometry, that is, for $r_{B\text{-}B} = r_{B\text{-}B,eq}$, this yields an expression for the bond energy $\Delta E(r_{B\text{-}B,eq}) = \Delta E = \Delta E_{strain} + \Delta E_{int}$. The interaction energy $\Delta E_{int}(r_{B\text{-}B})$ between the deformed reactants is further analyzed in the conceptual framework provided by the quantitative Kohn–Sham MO model.[50–51] To this end, it is decomposed into three physically meaningful terms [Equation (3)] using a quantitative energy decomposition analysis (EDA) as implemented in ADF.[50–53]

$$\begin{aligned}\Delta E_{int}(r_{B\text{-}B}) &= \Delta V_{elstat}(r_{B\text{-}B}) + \Delta E_{Pauli}(r_{B\text{-}B}) \\ &+\Delta E_{oi}(r_{B\text{-}B}) + \Delta E_{disp}(r_{B\text{-}B})\end{aligned} \tag{3}$$

The usually attractive term ΔV_{elstat} corresponds to the classical Coulomb interaction between the unperturbed charge distributions of the deformed reactants and has four components [Equation (4)]: (i) the electrostatic repulsion between the electron densities of fragments 1 and 2, $\Delta V_{elstat,p_1\rho_2}$; (ii) the electrostatic attraction between the nucleus of fragment 1 and the electron density of fragment 2, $\Delta V_{elstat,n_1\rho_2}$; (iii) the electrostatic attraction between the electron density of fragment 1 and the nucleus of fragment 2, $\Delta V_{elstat,p_1n_2}$; and (iv) the electrostatic repulsion between the nuclei of fragments 1 and 2, $\Delta V_{elstat,n_1n_2}$.

$$\begin{aligned}\Delta V_{elstat}(r_{B\text{-}B}) &= \Delta V_{elstat,p_1\rho_2}(r_{B\text{-}B}) + \Delta V_{elstat,n_1\rho_2}(r_{B\text{-}B}) \\ &+\Delta V_{elstat,p_1n_2}(r_{B\text{-}B}) + \Delta V_{elstat,n_1n_2}(r_{B\text{-}B})\end{aligned} \tag{4}$$

The Pauli repulsion energy (ΔE_{Pauli}) comprises the destabilizing interactions between the fully occupied orbitals on either fragment and arises from the antisymmetrization of the Hartree wavefunction due to the Pauli principle. The orbital-interaction energy (ΔE_{oi}) accounts for charge transfer, that is, the interaction between occupied orbitals of one fragment with unoccupied orbitals of the

other fragment, including the interactions of the highest occupied and lowest unoccupied MOs (HOMO-LUMO), and polarization, that is, empty-occupied orbital mixing on one fragment, due to the presence of another fragment. The dispersion energy ΔE_{disp} accounts for the dispersion corrections as introduced by Grimme et al.[36–37] To facilitate the analyses, the ASM and EDA were performed using the PyFrag 2019 program.[57–58]

Acknowledgements

We thank the Netherlands Organization for Scientific Research (NWO) for its support. This work was carried out on the Dutch national e-infrastructure with the support of SURF Cooperative. M.S. is grateful to financial support from the Spanish Ministerio de Ciencia e Innovación (project PID2020-113711GB-I00) and the Catalan Conselleria de Recerca i Universitats of the Generalitat de Catalunya (project 2021SGR623). D.E.T.G. thanks CONACyHT for a PhD fellowship (822937). Open access funding provided by the University of Girona.

Conflict of Interests

The authors declare no conflicts of interest.

Data Availability Statement

The data that support the findings of this study are available in the supplementary material of this article.

Keywords: Bond theory · Boron · Density functional calculations · Energy decomposition analysis · Multiple boron-boron bonds

[1] P. P. Power, *Nature* **2010**, *463*, 171–177.
[2] K. Chulsky, I. Malahov, D. Bawari, R. Dobrovetsky, *J. Am. Chem. Soc.* **2023**, *145*, 3786–3794.
[3] H. Braunschweig, I. Krummenacher, M.-A. Légaré, A. Matler, K. Radacki, Q. Ye, *J. Am. Chem. Soc.* **2017**, *139*, 1802–1805.
[4] W.-J. Tian, W.-J. Chen, M. Yan, R. Li, Z.-H. Wei, T.-T. Chen, Q. Chen, H.-J. Zhai, S.-D. Li, L.-S. Wang, *Chem. Sci.* **2021**, *12*, 8157–8164.
[5] M. Shibuya, M. Matsuda, Y. Yamamoto, *Chem. Eur. J.* **2021**, *27*, 8822–8831.
[6] M.-A. Légaré, C. Pranckevicius, H. Braunschweig, *Chem. Rev.* **2019**, *119*, 8231–8261.
[7] G. Berionni, *Chem. Synth.* **2021**, *1*, 10.
[8] D. W. Stephan, *J. Am. Chem. Soc.* **2015**, *137*, 10018–10032.
[9] D. W. Stephan, G. Erker, *Angew. Chem. Int. Ed.* **2015**, *54*, 6400–6441.
[10] T. A. Rokob, A. Hamza, I. Pápai, *J. Am. Chem. Soc.* **2009**, *131*, 10701–10710.
[11] G. C. Welch, R. R. S. Juan, J. D. Masuda, D. W. Stephan, *Science* **2006**, *314*, 1124–1126.
[12] M.-A. Légaré, M.-A. Courtemanche, É. Rochette, F.-G. Fontaine, *Science* **2015**, *349*, 513–516.
[13] J. Légaré Lavergne, A. Jayaraman, L. C. Misal Castro, É. Rochette, F.-G. Fontaine, *J. Am. Chem. Soc.* **2017**, *139*, 14714–14723.
[14] Y. Shao, J. Zhang, Y. Li, Y. Liu, Z. Ke, *Org. Lett.* **2018**, *20*, 1102–1105.
[15] M. Harhausen, R. Fröhlich, G. Kehr, G. Erker, *Organometallics* **2012**, *31*, 2801–2809.
[16] L. Greb, P. Oña-Burgos, B. Schirmer, S. Grimme, D. W. Stephan, J. Paradies, *Angew. Chem. Int. Ed.* **2012**, *51*, 10164–10168.
[17] M. Arrowsmith, J. Böhnke, H. Braunschweig, M. A. Celik, *Angew. Chem. Int. Ed.* **2017**, *56*, 14287–14292.
[18] M. Arrowsmith, J. Böhnke, H. Braunschweig, M. A. Celik, T. Dellermann, K. Hammond, *Chem. Eur. J.* **2016**, *22*, 17169–17172.
[19] J. Böhnke, T. Brückner, A. Hermann, O. F. González-Belman, M. Arrowsmith, J. O. C. Jiménez-Halla, H. Braunschweig, *Chem. Sci.* **2018**, *9*, 5354–5359.
[20] H. Braunschweig, T. Dellermann, R. D. Dewhurst, W. C. Ewing, K. Hammond, J. O. C. Jimenez-Halla, T. Kramer, I. Krummenacher, J. Mies, A. K. Phukan, A. Vargas, *Nat. Chem.* **2013**, *5*, 1025–1028.
[21] H. Zhang, Z. Cao, W. Wu, Y. Mo, *Angew. Chem. Int. Ed.* **2018**, *57*, 13076–13081.
[22] Y. Wang, B. Quillian, P. Wei, C. S. Wannere, Y. Xie, R. B. King, H. F. Schaefer, P. v. R. Schleyer, G. H. Robinson, *J. Am. Chem. Soc.* **2007**, *129*, 12412–12413.
[23] Y. Wang, B. Quillian, P. Wei, Y. Xie, C. S. Wannere, R. B. King, H. F. Schaefer, P. v. R. Schleyer, G. H. Robinson, *J. Am. Chem. Soc.* **2008**, *130*, 3298–3299.
[24] A. Hermann, M. Arrowsmith, D. E. Trujillo-Gonzalez, J. O. C. Jiménez-Halla, A. Vargas, H. Braunschweig, *J. Am. Chem. Soc.* **2020**, *142*, 5562–5567.
[25] H. Braunschweig, R. D. Dewhurst, K. Hammond, J. Mies, K. Radacki, A. Vargas, *Science* **2012**, *336*, 1420–1422.
[26] R. Borthakur, K. Saha, S. Kar, S. Ghosh, *Coord. Chem. Rev.* **2019**, *399*, 213021.
[27] J. Böhnke, H. Braunschweig, T. Dellermann, W. C. Ewing, T. Kramer, I. Krummenacher, A. Vargas, *Angew. Chem. Int. Ed.* **2015**, *54*, 4469–4473.
[28] J. Böhnke, H. Braunschweig, T. Dellermann, W. C. Ewing, K. Hammond, J. O. C. Jimenez-Halla, T. Kramer, J. Mies, *Angew. Chem. Int. Ed.* **2015**, *54*, 13801–13805.
[29] G. Frenking, N. Holzmann, *Science* **2012**, *336*, 1394–1395.
[30] D. E. Trujillo-González, G. González-García, T. A. Hamlin, F. M. Bickelhaupt, H. Braunschweig, J. O. C. Jiménez-Halla, M. Solà, *Eur. J. Inorg. Chem.* **2023**, *26*, e202200767.
[31] C. Xu, Y. Ma, L. Cheng, *J. Phys. Chem. A* **2021**, *125*, 1681–1687.
[32] K. Młodzikowska, A. A. Rajkiewicz, K. Grela, B. Trzaskowski, *New J. Chem.* **2018**, *42*, 6183–6190.
[33] E. v. Lenthe, E. J. Baerends, J. G. Snijders, *J. Chem. Phys.* **1993**, *99*, 4597–4610.
[34] A. D. Becke, *Phys. Rev. A* **1988**, *38*, 3098–3100.
[35] C. Lee, W. Yang, R. G. Parr, *Phys. Rev. B* **1988**, *37*, 785–789.
[36] S. Grimme, J. Antony, S. Ehrlich, H. Krieg, *J. Chem. Phys.* **2010**, *132*.
[37] S. Grimme, S. Ehrlich, L. Goerigk, *J. Comput. Chem.* **2011**, *32*, 1456–1465.
[38] I. Alkorta, J. E. Del Bene, J. Elguero, O. Mó, M. Yáñez, *Theor. Chem. Acc.* **2009**, *124*, 187–195.
[39] N. Holzmann, M. Hermann, G. Frenking, *Chem. Sci.* **2015**, *6*, 4089–4094.
[40] G. Verhaegen, J. Drowart, *J. Chem. Phys.* **2004**, *37*, 1367–1368.
[41] K.-P. Huber, *Molecular spectra and molecular structure: IV. Constants of diatomic molecules*, Springer Science & Business Media, New York, **2013**.
[42] V. Brites, C. Léonard, *Comput. Theor. Chem.* **2013**, *1025*, 24–29.
[43] B. Engels, H. U. Suter, M. Perić, *J. Phys. Chem.* **1996**, *100*, 10121–10122.
[44] M. Perić, S. D. Peyerimhoff, in *The role of Rydberg States in Spectroscopy and Photochemistry* (Ed.: C. Sándorfy), Kluwer Academic Publishers, Dordrecht, **1999**, pp. 137–178.
[45] M. Perić, B. Ostojić, B. Engels, *J. Mol. Spectrosc.* **1997**, *182*, 295–308.
[46] D. Schleier, A. Humeniuk, E. Reusch, F. Holzmeier, D. Nunez-Reyes, C. Alcaraz, G. A. Garcia, J.-C. Loison, I. Fischer, R. Mitric, *J. Phys. Chem. Lett.* **2018**, *9*, 5921–5925.
[47] E. Miliordos, A. Mavridis, *J. Chem. Phys.* **2008**, *128*, 144308.
[48] N. Holzmann, A. Stasch, C. Jones, G. Frenking, *Chem. Eur. J.* **2011**, *17*, 13517–13525.
[49] F. M. Bickelhaupt, J. K. Nagle, W. L. Klemm, *J. Phys. Chem. A* **2008**, *112*, 2437–2446.
[50] P. Vermeeren, T. A. Hamlin, F. M. Bickelhaupt, *Chem. Commun.* **2021**, *57*, 5880–5896.
[51] P. Vermeeren, S. C. C. van der Lubbe, C. Fonseca Guerra, F. M. Bickelhaupt, T. A. Hamlin, *Nat. Protoc.* **2020**, *15*, 649–667.
[52] F. M. Bickelhaupt, E. J. Baerends, in *Reviews in Computational Chemistry, Vol. 15* (Eds.: K. B. Lipkowitz, D. B. Boyd), Wiley-VCH, New York, **2000**, pp. 1–86.
[53] T. A. Hamlin, P. Vermeeren, C. Fonseca Guerra, F. M. Bickelhaupt, in *Complementary Bonding Analyses* (Ed.: S. Grabowski), De Gruyter, Berlin, **2021**, pp. 199–212.

[54] G. te Velde, F. M. Bickelhaupt, E. J. Baerends, C. Fonseca Guerra, S. J. A. van Gisbergen, J. G. Snijders, T. Ziegler, *J. Comput. Chem.* **2001**, *22*, 931–967.
[55] AMS 2023.1, SCM, Vrije Universiteit, Amsterdam, The Netherlands, http://www.scm.com, **2023**.
[56] E. van Lenthe, E. J. Baerends, J. G. Snijders, *J. Chem. Phys.* **1993**, *99*, 4597–4610.
[57] X. Sun, T. M. Soini, L. P. Wolters, W.-J. v. Zeist, C. Fonseca Guerra, T. A. Hamlin, F. M. Bickelhaupt, PyFrag 2007–2020, Vrije Universiteit Amsterdam, The Netherlands, **2020**.
[58] X. Sun, T. M. Soini, J. Poater, T. A. Hamlin, F. M. Bickelhaupt, *J. Comput. Chem.* **2019**, *40*, 2227–2233.

Manuscript received: September 29, 2023
Accepted manuscript online: October 23, 2023
Version of record online: December 15, 2023